

CONTROL OF STAR FORMATION IN GALAXIES BY GRAVITATIONAL INSTABILITY

YUEXING LI, MORDECAI-MARK MAC LOW

Department of Astronomy, Columbia University, New York, NY 10027, USA and
Department of Astrophysics, American Museum of Natural History, New York, NY 10024, USA

AND

RALF S. KLESSEN

Astrophysikalisches Institut Potsdam, An der Sternwarte 16, D-14482 Potsdam, Germany
Draft version October 30, 2019

ABSTRACT

We present high resolution simulations of star formation in a wide range of disk galaxies, using a three-dimensional smoothed particle hydrodynamics code with an isothermal equation of state and no explicit feedback. Absorbing sink particles are inserted in high density regions to directly measure the mass of gravitationally collapsing gas. Despite the simplicity of our assumptions, our models quantitatively reproduce not only observed global and local Schmidt laws, but also observed star formation thresholds in disk galaxies. Our results suggest that the dominant physical mechanism determining the star formation rate is just the strength of gravitational instability, with feedback primarily functioning to maintain a roughly constant effective sound speed.

Subject headings: galaxy: gravitational instability — galaxy: star formation — stars: formation

1. INTRODUCTION

Stars form in galaxies at hugely varying rates (Kennicutt 1998a). The mechanisms that control the rate of star formation from interstellar gas are widely debated (Shu et al. 1987; Elmegreen 2002; Larson 2003; Mac Low & Klessen 2004). Gravitational collapse is opposed by gas pressure, supersonic turbulence, magnetic fields, and rotational shear. Gas pressure in turn is regulated by radiative cooling and stellar and turbulent heating. Despite this complexity, star-forming spiral galaxies follow two simple empirical laws. First, stars only form above a critical gas surface density (Martin & Kennicutt 2001) that appears to be determined by the Toomre criterion for gravitational instability (Toomre 1964). Second, the rate of star formation is proportional to a power of the total gas surface density (Kennicutt 1998b), as first proposed by Schmidt (1959).

The importance of gravitational instability in controlling large-scale star formation was emphasized by Elmegreen (2002). Friedli & Benz (1995) used low resolution (10^4 gas particles) models of galaxies lacking dark matter to argue that Schmidt laws followed from the Toomre criterion. A similar conclusion comes from the observation that thin dust lanes in galaxies only form in gravitationally unstable regions (Dalcanton et al. 2004). Recent cosmological simulations by Kravtsov (2003) agree, and suggest little contribution from feedback.

In order to investigate gravitational instability in disk galaxies and consequent star formation, we model a large set of galaxies composed of a dark matter halo and a disk of stars and isothermal gas, using high resolution (5×10^5 gas particles or more), three-dimensional, smoothed particle hydrodynamics (SPH) simulations. The galaxy models cover a wide range of rotational velocity, gas fraction, and initial gravitational instability. In this Letter, we compare the Schmidt laws and star formation thresh-

olds we derive from our simulations to the observations. In § 2 we briefly describe the computational method. The global and local Schmidt laws are presented in §3 and §4, respectively. The star formation threshold is demonstrated in §5. In §6 we discuss the correlation between star formation and gravitational instability, and the implications of our work for star formation and evolution in various types of galaxies.

2. COMPUTATIONAL METHOD

We here summarize our computational method. Details will be given in subsequent work. We use the SPH code GADGET (Springel et al. 2001), modified to include absorbing sink particles (Bate et al. 1995) to directly measure the mass of gravitationally collapsing gas. Sink particles, representing proto-star clusters (PSCs), are inserted in gravitationally bound regions with densities $n > 10^3 \text{ cm}^{-3}$ following Bromm & Clarke (2002).

Our galaxy model consists of a dark matter halo, and a disk of stars and isothermal gas. The galaxy structure is based on the analytical work by Mo et al. (1998), as implemented numerically by Springel & White (1999) and Springel (2000). The isothermal sound speed is chosen to be either $c_1 = 6 \text{ km s}^{-1}$ in low temperature (LT) models or $c_2 = 15 \text{ km s}^{-1}$ in high temperature (HT) models. Table 1 lists the most important model parameters. The Toomre criterion for gravitational instability that couples stars and gas, Q_{sg} is calculated according to equations (27–30) in Rafikov (2001), and the minimum is derived at minimum wavenumber k .

The gas, halo and disk particles are distributed with number ratio $N_g : N_h : N_d = 5 : 3 : 2$. The gravitational softening lengths of the halo $\epsilon_h = 0.4 \text{ kpc}$ and disk $\epsilon_d = 0.1 \text{ kpc}$, while the softening length of the gas ϵ_g is given in Table 1 for each model. We adopt typical values for the halo concentration parameter $C = 5$, spin parameter $\lambda = 0.05$, and Hubble constant $H_0 = 70 \text{ km s}^{-1} \text{ Mpc}^{-1}$ (Springel 2000).

Our models must satisfy three numerical criteria to

TABLE 1
GALAXY MODELS AND NUMERICAL PARAMETERS

Model ^a	f_g ^b	$Q_{sg}(LT)$ ^c	$Q_{sg}(HT)$ ^d	N_{tot} ^e	ϵ_g ^f	m_g ^g
G50-1	1	1.22	1.45	1.0	0.01	0.08
G50-2	2.5	0.94	1.53	1.0	0.01	0.21
G50-3	4.5	0.65	1.52	1.0	0.01	0.37
G50-4	9	0.33	0.82	1.0	0.01	0.75
G100-1	1	1.08	1.27	1.0	0.01	0.66
G100-2	2.5	0.57	1.07	1.0	0.01	1.65
G100-3	4.5	0.33	0.82	1.0	0.01	2.97
G100-4	9	0.17	0.42	1.0	0.02	5.94
G120-3	4.5	0.28	0.68	1.0	0.02	5.17
G120-4	9	0.14	0.35	1.0	0.03	10.3
G160-1	1	0.85	1.34	1.0	0.02	2.72
G160-2	2.5	0.37	0.89	1.0	0.02	6.80
G160-3	4.5	0.21	0.52	1.0	0.03	12.2
G160-4	9	0.11	0.26	1.5	0.04	16.3
G220-1	1	0.65	1.11	1.0	0.02	7.07
G220-2	2.5	0.27	0.66	1.2	0.03	14.8
G220-3	4.5	0.15	0.38	2.0	0.04	15.9
G220-4	9	0.08	0.19	4.0	0.04	16.0

^aFirst number gives rotational velocity V_c in km s^{-1} at virial radius.

^bPercentage of total halo mass in gas.

^cMinimum initial Q_{sg} for LT model

^dMinimum initial Q_{sg} for HT model

^eTotal particle number in millions for HR runs.

^fGravitational softening length of gas in kpc.

^gGas particle mass in units of $10^4 M_\odot$.

follow collapse to sink-particle densities. These are the Jeans resolution criterion (Bate & Burkert 1997; Whitworth 1998), the gravity-hydro balance criterion for gravitational softening (Bate & Burkert 1997), and the equipartition criterion for particle masses (Steinmetz & White 1997). We carried out a total of 54 simulations, including two sets of high resolution (HR) runs with LT and HT sound speeds that not only fully satisfy the three criteria but also have $N_{tot} \geq 10^6$ particles; and one set of low-resolution (LR), HT runs with $N_{tot} = 10^5$, not meeting all criteria simultaneously. The minimum spatial and mass resolutions in the gas are given by the gravitational softening length ϵ_g and twice the kernel mass ($\sim 80m_g$).

3. GLOBAL SCHMIDT LAW

The relationship between surface densities of star formation rate Σ_{SFR} and gas density Σ_{gas} can be integrated over entire galaxies, giving a global Schmidt law. We define the radius of the star forming region to encircle 80% of the newly formed PSCs. The SFR is measured from gas accreted into PSCs, assuming a local star formation efficiency of 35%. Figure 1 shows the global Schmidt law derived from our simulations. The best fit to the observations by Kennicutt (1998b) gives $\Sigma_{SFR} = (2.5 \pm 0.7) \times 10^{-4} \Sigma_{gas}^{1.4 \pm 0.15}$, where Σ_{SFR} is given in units of $M_\odot \text{ kpc}^{-2} \text{ yr}^{-1}$, while Σ_{gas} is given in units of $M_\odot \text{ pc}^{-2}$. A least-squares fit to the HR models (both LT and HT) gives $\Sigma_{SFR} = (1.8 \pm 0.6) \times 10^{-4} \Sigma_{gas}^{1.49 \pm 0.07}$, agreeing surprisingly well with the observations.

If we just fit to the HR, LT models we find $\Sigma_{SFR} = (2.1 \pm 0.4) \times 10^{-4} \Sigma_{gas}^{1.54 \pm 0.04}$, while the HR, HT models give $\Sigma_{SFR} = (0.7 \pm 0.3) \times 10^{-4} \Sigma_{gas}^{1.56 \pm 0.1}$, which has the same slope within errors, but is several standard devia-

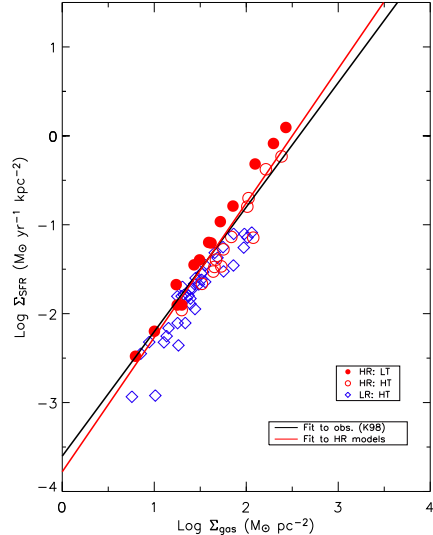


FIG. 1.— Global Schmidt law from HR, LT models (red filled circles), and HT models at high (red open circles), and low (blue diamonds) resolution. The black line is the best fit to the observation from Kennicutt (1998b), the red line is the best fit to all HR models (both LT and HT).

tions different in normalization. Thus, existing observations seem already to measure the effective sound speed (roughly equivalent to velocity dispersion) of the star-forming gas in galactic disks and nuclei to within a factor of two. Star-formation rates for individual models in LR and HR cases differ substantially. In future work we will show the agreement between models satisfying the three numerical criteria but with resolutions differing by a factor of eight in mass. The Schmidt law derived from our LR models does however agree within the errors with the HR models with the same parameters, demonstrating that at least this result has converged sufficiently well.

Our chosen models do not populate the lowest and highest star formation rates observed. Interacting galaxies can produce disks even more unstable than our most unstable disks, while quiescent normal galaxies form stars at a rate below our mass resolution limit. Indeed our most stable models show no star-cluster formation in the first few Gyrs.

4. LOCAL SCHMIDT LAW

The relationship between Σ_{SFR} and Σ_{gas} can also be measured as a function of position within a galaxy, giving a local Schmidt law. Figure 2 (*top*) shows examples from models G220-1, G220-3, and G220-4. Each galaxy is divided into 40 radial annuli within $4R_d$, the radial disk scale length, and the average Σ_{gas} and Σ_{SFR} is computed in each annulus. Below some gas surface density, a tail is clearly seen where the star formation rate drops dramatically, clear evidence of a star formation threshold. The density threshold is different from galaxy to galaxy. Big galaxies have higher density threshold than small ones, while for galaxies with the same rotational velocity, gas-rich models have higher threshold density than gas-poor ones. We define the threshold radius R_{th} as the radius that encircles 95% of the newly formed

PSCs. The blue and red lines are fits to data within R_{th} , giving $\Sigma_{\text{SFR}} = (0.28 \pm 0.16) \times 10^{-4} \Sigma_{\text{gas}}^{1.54 \pm 0.18}$ for G220-1, and $\Sigma_{\text{SFR}} = (29 \pm 11) \times 10^{-4} \Sigma_{\text{gas}}^{1.22 \pm 0.19}$ for the most gas rich model G220-4. We can see that their normalizations vary substantially. Gas rich models have larger normalization, suggesting higher global star formation efficiency. The slope of the fits also varies from galaxy to galaxy. Figure 2 (*bottom*) shows the power law indices α for all HR, LT models. Open symbols are fits to all points, while filled symbols include only points within R_{th} . We can see that there is substantial variation in the indices, as is observed (e.g. Heyer et al. 2004), but their average slope agrees with the global Schmidt law.

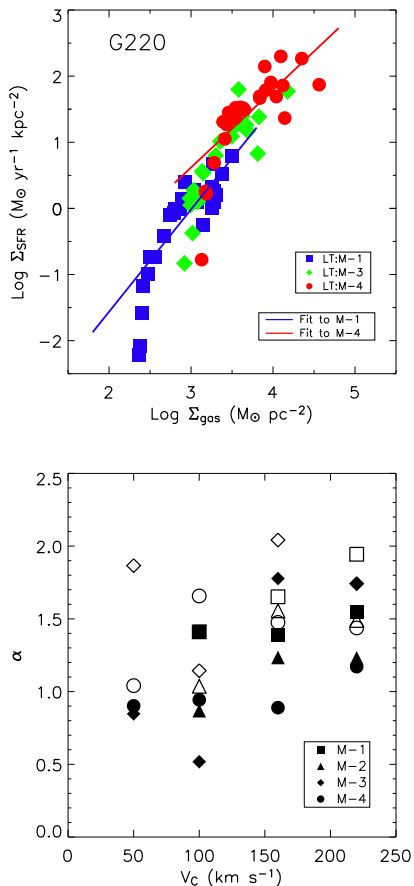


FIG. 2.— (*Top*) Local Schmidt laws demonstrated by G220, submodels 1 (*blue squares*), 3 (*green diamonds*), and 4 (*red circles*). The blue and red lines are fits to points within R_{th} of G220-1 and G220-4, respectively. (*Bottom*) Power law indices for all HR, LT models. Open symbols are fits to all points, filled symbols include only points within R_{th} .

5. STAR FORMATION THRESHOLD

A threshold is clearly visible in the spatial distribution of gas and stars in our galaxy models, as illustrated by model G220-1 in Figure 3 (*top*). The critical value of instability parameters at threshold can be quantitatively measured from their radial profiles as shown in *middle panel*, which shows a sharp drop of Σ_{SFR} at $R \sim 2R_{\text{d}}$. The critical values of Q_{sg} and Q_{g} at threshold R_{th} are shown in Figure 3 (*bottom*) for all the HR, LT models.

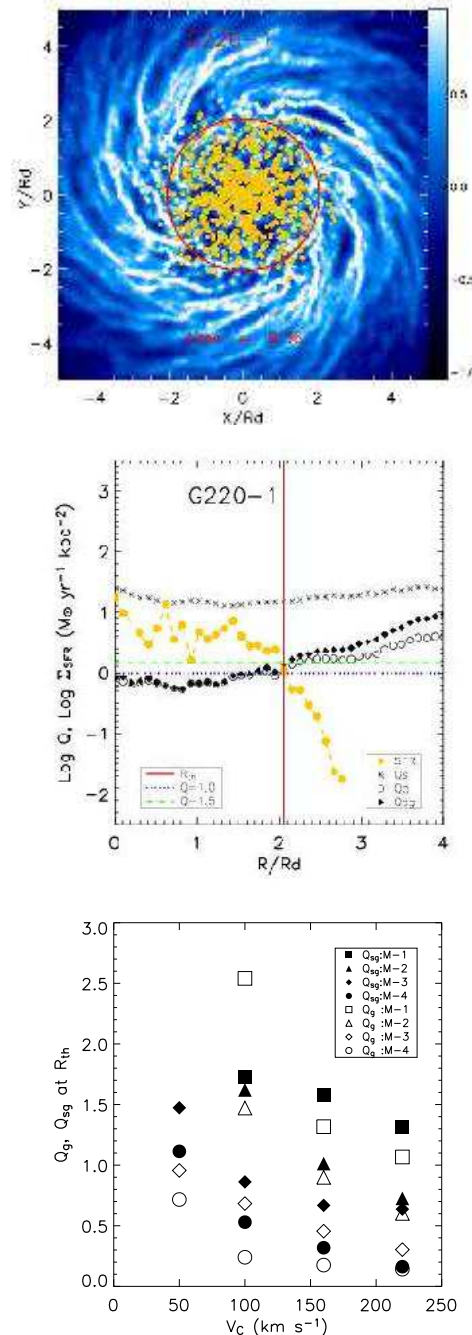


FIG. 3.— (*Top*) Star formation threshold illustrated by model G220-1. Log of gas surface density is shown, with values given by the color bar. Yellow dots indicated PSCs, while the red circle shows R_{th} . (*Middle*) Radial profiles of SFR (yellow circles), and Toomre Q parameters for stars Q_{s} (asterisks), gas Q_{g} (circles), and stars and gas combined Q_{sg} (diamonds). The red line shows R_{th} . (*Bottom*): critical values of Q_{sg} (filled symbols) and Q_{g} (open symbols) at R_{th} for all HR, LT models, as described in key.

We can see that the critical Q_{sg} is generally higher than the critical Q_{g} in the same galaxy, and they have lower values (< 1) in more unstable models.

Most galaxies not classified as starbursts have gas fractions comparable to or less than our most stable mod-

els, so the observation of a threshold value of $Q_g \sim 1.4$ may reflect the stability of the galaxies in the sample (Martin & Kennicutt 2001). Observed variations in the threshold also appear to occur naturally. If we only use the Toomre criterion for the gas Q_g we get slightly larger scatter than if we include the stars and use the combined criterion Q_{sg} , but the effect is small.

6. DISCUSSION AND SUMMARY

What is the physical cause of the star formation behavior that we see in our different galaxy models? The most obvious candidate is the nonlinear development of gravitational instability. Figure 4 shows the correlation between the star formation timescale τ_{SF} and the initial minimum $Q_{sg}(min)$ for all HR, LT (filled symbols) and HT (open symbols) models. The solid line is the least-square fit, which gives $\tau_{SF} = (60 \pm 9 \text{ Myr}) \times \exp[(3.1 \pm 0.2)Q_{sg}(min)]$. Quiescent star formation occurs where Q_{sg} is large, while vigorous starbursts occur where Q_{sg} is small. Typical observed starburst times of 10^8 yr are consistent with our fit for τ_{SF} . Star formation begins when the gas become unstable, with rate controlled by $Q_{sg}(min)$. Galaxies with high mass or gas fraction are the most unstable, forming stars quickly.

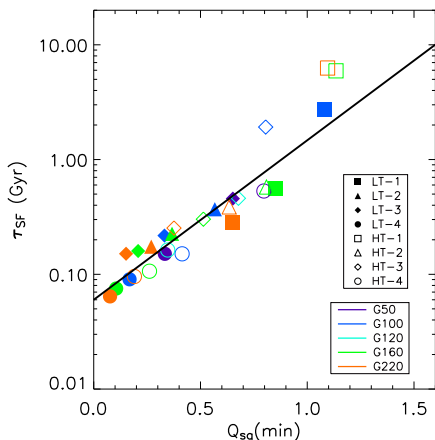


FIG. 4.— Star formation timescale τ_{SF} as a function of initial $Q_{sg}(min)$, for all high-resolution LT (*filled symbols*) and HT (*open symbols*) models. The solid line is the least-square fit.

The assumption of an isothermal equation of state for

the gas implies substantial feedback to maintain the effective temperature of the gas against radiative cooling and turbulent dissipation. Real interstellar gas has a wide range of temperatures. However, the rms velocity dispersion generally falls within the range 6 - 12 km s^{-1} (e.g. Elmegreen & Scalo 2004). Direct feedback from the starburst may play a minor role in quenching subsequent star formation, perhaps because most energy is deposited not in the disk but above it as superbubbles blow out. We have neglected magnetic fields and explicit feedback in our models. Kim & Ostriker (2001) demonstrate that swing and magneto-Jeans instabilities operating in a gaseous disk occur at $Q_g \sim 1.4$, suggesting that magnetostatic support is unimportant.

In summary, we have derived the global and local Schmidt laws, as well as star formation thresholds from our simulations. The remarkable agreement between simulations and observations suggests that gravitational instability in effectively isothermal gas may be the dominant physical mechanism that controls the rate and location of star formation in different galaxies. Unstable galaxies were more common at early cosmic times, so our results, together with merger-induced starbursts, may account for the Butcher-Oemler effect (Butcher & Oemler 1984) of increasing blueness of galaxies with redshift. We find that massive galaxies form stars quickly, which may account for the downsizing effect that star formation first occurs in big galaxies at high redshift, while modern starburst galaxies are small (Cowie et al. 1996; Poggianti et al. 2004). The slow evolution of star formation in our low mass models resembles that observed in low surface brightness galaxies (van den Hoek et al. 2000).

We thank V. Springel for making both GADGET and his galaxy initial condition generator available, as well as for useful discussions, A.-K. Jappsen for participating in the implementation of sink particles in GADGET, and F. Adams, J. Dalcanton, R. Kennicutt, J. Lee, C. Martin, D. McCray, T. Quinn, M. Shara, and J. van Gorkom for useful discussions. This work was supported by the NSF under grants AST99-85392 and AST03-07854, by NASA under grant NAG5-13028, and by the DFG under grant KL1358/1. Computations were performed at the Pittsburgh Supercomputer Center supported by the NSF, on the Parallel Computing Facility of the AMNH, and on an Ultrasparc III cluster generously donated by Sun Microsystems.

REFERENCES

- Bate, M. R., Bonnell, I. A., & Price, N. M. 1995 MNRAS 277, 362
 Bate, M. R. & Burkert, A. 1997 MNRAS 288, 1997
 Bromm, V. & Clarke, C. 2002 ApJ 566, 1
 Butcher, H. & Oemler, A., Jr. 1984 ApJ 285, 426
 Cowie, L. L. et al. 1996 AJ 112, 839
 Dalcanton, J., Yoachim, P. & Bernstein, R. A. 2004 ApJ 608, 189
 Elmegreen, B. G. 2002 ApJ 577, 206
 Elmegreen, B. G., & Scalo, J. 2004 ARAA, in press (astro-ph/0404451)
 Friedli, D. & Benz, W. 1995 A&A 301, 649
 Heyer, M. H. et al. 2004 ApJ 602, 723
 Kennicutt, R. C., Jr. 1989, ApJ 344, 685
 Kennicutt, R. C., Jr. 1998, ARA&A 36, 189
 Kennicutt, R. C., Jr. 1998, ApJ 498, 541
 Kim, W.-T., & Ostriker, E. C. 2001 ApJ 559, 70
 Kravtsov, A. V. 2003 ApJL 590, 1
 Larson, R. B. 2003 Rep. Prog. Phys. 66, 1651
 Mac Low, M.-M. & Klessen, R. S. 2004 Rev. Mod. Phys. 76, 125
 Martin, C. L. & Kennicutt, R. C. Jr. 2001 ApJ 555, 301
 Mo, H. J., Mao, S., & White, S. D. M. 1998 MNRAS 295, 319
 Poggianti, B. M. et al. 2004 ApJ 601, 197
 Rafikov, R. R. 2001 MNRAS 323, 2001
 Schmidt, M. 1959 ApJ 129, 243
 Shu, F., Adams, F. C. & Lizano, S. 1987 ARA&A 25, 23
 Springel, V. 2000 MNRAS 312, 859
 Springel, V. & White, S. M. D. 1999 MNRAS 307, 162
 Springel, V., Yoshida, N. & White, S. D. M. New Astron. 6, 79
 Steinmetz, M. & White, S. D. M. 1997 MNRAS 288, 545
 Toomre, A. 1964 ApJ 139, 1217
 van den Hoek, L. B. et al. 2000 ApJ 357, 397

